Efficient Voltage-Driven Oxidation of Water and Alcohols by Organic Molecular Catalyst Directly Attached to a Carbon Electrode

Koushik Barman,[†] Gaukhar Askarova, [†,§] Rui Jia,[†,§] Guoxiang Hu,[†,§,*] and Michael V. Mirkin[†,#,*]

† Department of Chemistry and Biochemistry, Queens College-CUNY, Flushing, NY 11367, USA.

§ The Graduate Center of CUNY, New York, NY 10016.

Advanced Science Research Center at The Graduate Center, CUNY; New York, NY 10031.

Corresponding Author

E-mail: guoxiang.hu@qc.cuny.edu, mmirkin@qc.cuny.edu

ABSTRACT

The integration of heterogeneous electrocatalysis and molecular catalysis is a promising approach to designing new catalysts for oxygen evolution reaction (OER) and other processes. We recently showed that the electrostatic potential drop across the double layer contributes to the driving force for electron transfer between a dissolved reactant and a molecular catalyst immobilized directly on the electrode surface. Here we report high current densities and low onset potentials for water oxidation attained using a metal-free voltage-assisted molecular catalyst (TEMPO). Scanning electrochemical microscopy (SECM) was used to analyze the products and determine faradaic efficiencies for the generation of H_2O_2 and O_2. The same catalyst was employed for efficient oxidations of butanol, ethanol, glycerol, and H_2O_2. DFT calculations show that the applied voltage alters the electrostatic potential drop between TEMPO and the reactant as well as chemical bonding between them, thereby increasing the reaction rate. These results suggest a new route for designing next-generation hybrid molecular/electrocatalysts for OER and alcohol oxidations.

INTRODUCTION

The progress in alternative energy and solar fuel technology requires the development of efficient catalysts for several electrochemical processes, including oxidations of water[1,2] and alcohols.[3] The catalysis of multi-electron, multi-proton oxygen evolution reaction (OER) is especially challenging. A typical molecular catalyst for OER is a reversible redox mediator whose standard potential is sufficiently positive to oxidize water.[4-7] Typically based on transition-metal complexes, such catalysts are either homogeneous (i.e., dispersed in electrolyte solution)[8-20] or heterogeneous (i.e., immobilized on the electrode surface).[21-30] In addition to a very low load and ease of recycling, surface attachment of some molecular catalysts has improved their activities.[21-23] Despite potential advantages of metal-free, fully organic OER catalysts, only a few of them have been reported to date.[31-34] A high standard potential required for water oxidation limits the choice of suitable organic molecular catalysts. Another problem is the decomposition of organic and organometallic water-oxidation catalysts at high anodic potentials.[35]

Unlike molecular catalysis of water oxidation, electrocatalytic OER occurs on active surface sites and is driven by the applied electrode potential.[7,36] Despite extensive research, various issues, including high cost, surface passivation, high overpotentials, and complex engineering and characterization of active sites, hinder commercial applications of OER electrocatalysts. Recent studies focused on the advantages of combining molecular catalysts and electrocatalysts into hybrid systems for OER[7,37-40] and other processes. Direct coupling of catalysts to carbon electrodes reported by the Surendranath group produced tunable heterogeneous catalysts with molecularly well-defined active sites.[41-43] The molecules conjugated to carbon became part of the electrode, so that no electron transfer (ET) occurred

between the electrode and a catalytic moiety whose oxidation state remained unchanged.[43] The same group reported solvent-dependent ET behavior, where major changes to electrostatic coupling between the molecule and the surface were induced by the change of the solvent.[44] Thus, cobalt tetraphenylporphyrin attached to a carbon electrode by an aliphatic linkage operated as a regular redox mediator in acetonitrile and as a part of the electrode in aqueous media.

We showed recently that the potential drop across the electrical double layer (EDL) can contribute to the driving force for ET between a molecular catalyst immobilized directly on the electrode surface and a dissolved reactant.[45] Specifically, a fraction of the applied potential dropping between the electrode and the attached molecular catalyst causes its oxidation/reduction, while the other fraction of the applied potential dropping between the attached molecular catalyst and the dissolved reactant drives the electrocatalytic process (Fig. 1A). Distinct from conventional molecular catalysis or electrocatalysis, here the electrostatic potential drop across the EDL is distributed on both sides of the attached molecular catalyst. An important corollary for OER is that the additional driving force derived from the applied electrode potential can enable the use of a molecular catalyst with a standard potential lower than that normally required for water oxidation. Here, we report voltage-driven molecular catalysis of water oxidation by TEMPO (2,2,6,6-tetramethyl-1-piperidine N-oxyl; a fully organic molecular catalyst extensively employed for electrosynthesis[46,47]) immobilized either on a carbon nanoelectrode (CNE; see Experimental Section) or a macroscopic glassy carbon disk electrode (GCE; Fig. S1) surface. By contrast, homogeneous catalysis of water oxidation by TEMPO does not occur. Pulse radiolysis and spectroelectrochemical studies identified the formation of TEMPO-OH (a hydroxide adduct of $TEMPO^+$) at high pH values.[48,49] Thus, we anticipate that inner-sphere ET (rather than voltage-assisted outer-sphere ET reported in ref. 45) occurs between

$TEMPO^+$ and OH^- coincident with the chemical bond formation (Fig. 1B).

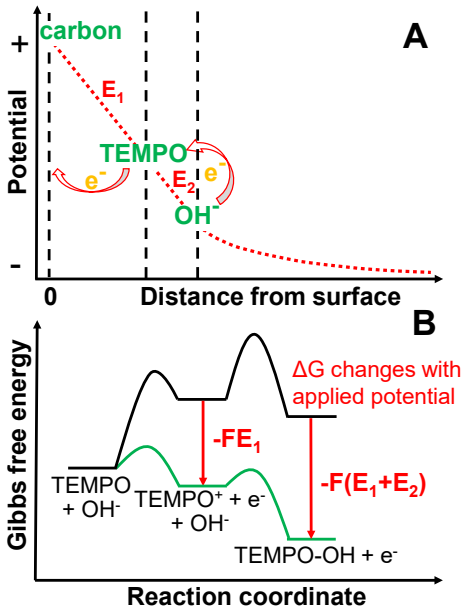

Fig. 1. Voltage-driven catalysis of water oxidation by TEMPO molecules directly attached to the carbon surface. (A) Scheme of the potential drop (red dotted line) across the carbon electrode/solution interface. A fraction of the applied potential drops between the surface-attached TEMPO and dissolved OH^-. (B) Hypothesized free energy diagram.

Other significant examples of voltage-assisted molecular catalysis by surface-attached TEMPO are oxidations of primary alcohols (ethanol and n-butanol) and an important biofuel (glycerol). The mechanism of TEMPO-catalyzed electrooxidation involves the formation of an adduct between $TEMPO^+$ and alcohol, followed by the rate-determining intramolecular hydrogen transfer that yields TEMPOH and the organic carbonyl.[47] Our density functional theory (DFT) calculations suggest that the applied voltage can decrease the reaction free energy for this step, thereby increasing the reaction rate.

RESULTS & DISCUSSION

Voltage-driven water oxidation catalysis by TEMPO. The direct attachment (i.e., without a spacer) of the redox mediator to the electrode surface is required for voltage-driven

molecular catalysis.[45] Reagent-free covalent attachment of TEMPO to the carbon surface via anodic oxidation of 4-NH_2-TEMPO in aqueous solution has been reported previously[50] (see Experimental Section). This procedure produces a monolayer/sub-monolayer through the covalent linkage to the carbon surface rather than multilayers because there are no unsaturated sites in the TEMPO molecule, and no bond formation/attachment can occur between the surface bound TEMPO species and a dissolved NH_2-TEMPO molecule.[51] Cyclic voltammograms (CVs; Fig. 2A) of TEMPO directly attached to the surface of a 3-mm-diameter GCE in 0.1 M phosphate buffer saline (PBS) at pH 7 show a pair of anodic/cathodic peaks with the mid-peak potential, $E \approx 0.56$ V vs Ag/AgCl reference (for immobilized TEMPO this value is essentially independent of pH[51]) and the background-subtracted peak current directly proportional to the potential sweep rate (the inset in Fig. 2A). The mid-peak potential is ~120 mV more positive than that measured with TEMPO dissolved in the same electrolyte solution (0.44 V vs. Ag/AgCl; Fig. S2). The surface coverage value, $\Gamma_{TEMPO} = 13.8$ pmol/cm^2 obtained from CVs by integrating the area under the oxidation peak after background subtraction. This value corresponds to <10% of the full monolayer coverage. (The monolayer coverage of TEMPO is ~2 x 10^{-10} mol/cm^2.[52])

A CV obtained at the TEMPO-modified GCE in 0.1 M KOH (curve 2 in Fig. 2B) shows the water oxidation current much higher than that measured at the bare GCE (curve 3; the current at the bare GCE may be due to carbon oxidation or other oxidation processes). The corresponding Tafel plot obtained from a slow-scan voltammogram (v = 5 mV/s) is shown in Fig. S3A. The overpotential required to attain for 0.1 mA/cm^2 current density is about 450 mV lower at a TEMPO-GCE than at a bare GCE. The water oxidation current is even higher in 0.2 M KOH (curve 1). By contrast, the reported CVs of aqueous solutions containing TEMPO show no signs of homogeneous water oxidation catalysis at any pH (i.e., $5 \leq pH \leq 13$ [53]).

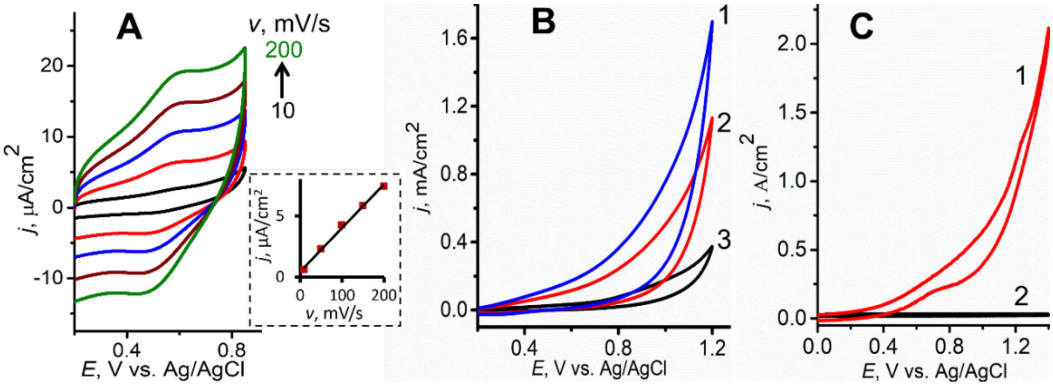

Fig. 2. Water oxidation catalysis by TEMPO. (A) CVs of TEMPO-modified GCE at different potential sweep rates (v) in pH 7 PBS solution. v, mV/s = 10 (black curve), 50 (red), 100 (blue), 150 (brown), and 200 (green). Inset: scan rate dependence of the anodic peak current. (B) Water oxidation at the TEMPO-modified GCE in 0.2 M KOH (1) and 0.1 M KOH (2). Curve 3 was obtained at a bare GCE in 0.1 M KOH. v = 20 mV/s. (C) Voltammograms of water oxidation at the TEMPO-modified (1) and bare (2) 50-nm-radius CNE in 0.1 M KOH. v = 5 mV/s.

TEMPO attached to the surface of a CNE (TEM image shown in Fig. S4A) exhibits a much faster apparent rate of catalytic OER with the current density reaching >2 A/cm^2 (curve 1 in Fig. 2C). These very high apparent current density values are calculated using the geometrical surface area (πa^2, where a is the nanodisk radius) rather than the true surface area, which is very hard to evaluate for a porous nanoelectrode. The true surface area of the porous carbon exposed to the solution is much larger than the geometrical surface area.[45,54] The current onset at ~0.4 V corresponds to the beginning of TEMPO oxidation ($E^{\circ}_{O_2/H_2O}$ = 0.253 V vs. Ag/AgCl at pH13), which is supposed to be complete at $E \approx 0.6 - 0.7$ V. At more positive CNE potentials, the current continues to increase over a wide potential range (~700 mV), which cannot be attributed to direct oxidation of water on the bare CNE surface because the current produced by this process (curve 2 in Fig. 2C) is orders of magnitude lower than that in curve 1. This behavior characteristic of voltage-driven molecular catalysis[45] is radically different from conventional

molecular catalysis in which the anodic current should reach a plateau when the applied potential becomes sufficiently positive for complete oxidation of surface-bound mediator species.[4] The steady-state current at TEMPO-modified CNE (Fig. S4B, curve 1) is ~15 times higher than that recorded at a similarly sized bare CNE (curve 2), suggesting that TEMPO catalyzed water oxidation rather than the oxidation of carbon is the main source of currents measured at nanoelectrodes.

The water oxidation process at TEMPO-modified carbon electrodes is likely going through the $2e^-$ H_2O_2 formation followed by its oxidation to O_2, as reported earlier for two other organic catalysts, N(5)-ethylflavinium ion[31] and pyridine-N-oxyl radical.[34] We used the substrate generation/tip collection (SG/TC; Fig. 3) mode of scanning electrochemical microscopy (SECM) to quantify the products and evaluate faradaic efficiency for the processes occurring during the water oxidation at TEMPO-GCE.

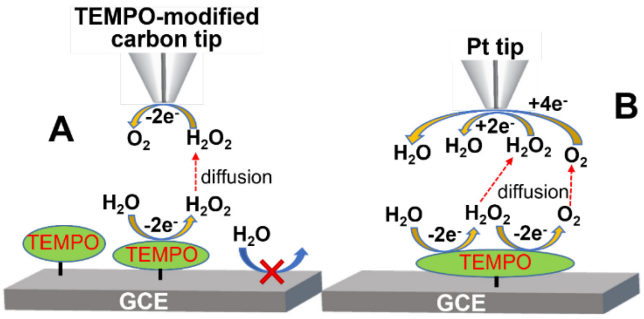

Fig. 3. Schematic representation of substrate generation/tip collection (SG/TC) SECM measurements of voltage-driven water oxidation by TEMPO. (A) H_2O_2 produced by water oxidation at the substrate is oxidized at the tip. (B) H_2O_2 produced by water oxidation at TEMPO-GCE can either diffuse away from the substrate surface or get further oxidized to produce O_2. Both water oxidation products are reduced at the tip. No water oxidation occurs at the catalytically inert carbon surface.

In two types of SECM experiments (Fig. 3) a TEMPO-modified GCE was used as a substrate electrode in 0.1 M KOH solution. Two tip current vs. time (i_T-t) curves (Fig. 4A) were obtained at a TEMPO-modified 3.5-µm-radius carbon fiber SECM tip positioned 5 µm above the substrate surface and biased at E_T = 0.8 V vs. Ag/AgCl to oxidize H_2O_2 and/or water. Curve 1 was recorded with the substrate biased at E_S = 0.2 V vs. Ag/AgCl at which no oxidation of water occurred at TEMPO-GCE, and i_T = 3.18 nA was only due to water oxidation at the tip.

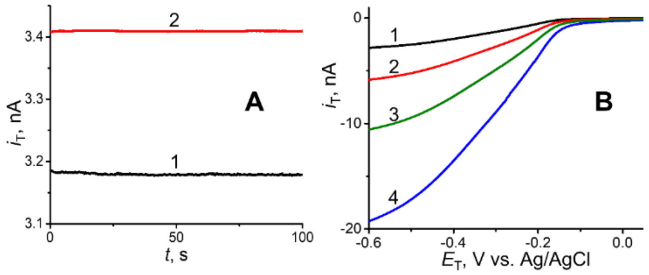

Fig. 4. Probing water oxidation at the TEMPO-GCE substrate with SECM. (A) i_T-t curves were obtained with a 3.5-µm-radius TEMPO-modified carbon fiber tip positioned 5 µm above the substrate surface. E_S, V vs. Ag/AgCl = 0.2 (1) and 1.2 (2). E_T = 0.8 V. (B) Voltammograms recorded at a 5-µm-radius Pt tip positioned 5 µm above the TEMPO-GCE surface at different substrate potentials. E_S, V = 0.2 (1), 0.6 (2), 1.0 (3), and 1.2 (4).

In curve 2 (Fig. 4A), the E_S is changed to 1.2 V to oxidize water, and the increased i_T = 3.41 nA comprises two components, i.e., the water oxidation current (3.18 nA, same as in curve 1) and the current due to the oxidation of H_2O_2 generated at the TEMPO-GCE (0.23 nA). Because the H_2O_2 oxidation current at the tip is kinetic (rather than diffusion limited), the response factor is required for the data analysis. The tip response to H_2O_2 was calibrated in 0.1 M KOH solutions containing different peroxide concentrations (Fig. S5). Finite-element simulations (Supporting Information) were carried out to evaluate the component of the substrate current associated with the H_2O_2 generation from the measured i_T. From this value (1.76 µA) and the total substrate current (32 µA), the faradaic efficiency for the generation of H_2O_2 at the

TEMPO-GCE surface is 5.5%.

Whereas homogeneous catalysis of hydrogen peroxide oxidation by TEMPO is very slow,[55] CNE-bound TEMPO exhibits significant activity for voltage-assisted oxidation of H_2O_2 (Fig. S6). Thus, TEMPO catalyzed water oxidation is expected to produce a significant amount of O_2 in addition to H_2O_2. In the second SECM experiment (Fig. 3B), the tip potential was swept in the negative direction (from 0 to -0.6 V vs. Ag/AgCl) to reduce both H_2O_2 and O_2 generated at the TEMPO-GCE substrate. Curve 1 in Fig. 4B was obtained at E_S = 0.2 V vs. Ag/AgCl at which no oxidation of water occurred at TEMPO-GCE, and i_T was only due to the reduction of dissolved oxygen at the Pt tip. The tip current increased with increasing E_S (curves 2-4 in Fig. 4B) due to the larger fluxes of H_2O_2 and O_2 generated at the substrate. At E_S = 1.2 V (curve 4), the component of the substrate current associated with the H_2O_2 generation is the same as in Fig. 4A (1.76 μA), and the tip current at E_T = -0.6 V (i_T = 19.5 nA) is due to the reduction of both H_2O_2 and O_2. Using this i_T value, the component of the substrate current associated with the O_2 generation was evaluated by COMSOL simulations. From this value (18.9 μA) and the total substrate current (32 μA), the faradaic efficiency for the generation of O_2 at the TEMPO-GCE surface is 54.04%, which is significantly higher than the values reported in refs. 31 and 34 (30% and 25.8%, respectively) for other organic water oxidation electrocatalysts. The total faradaic efficiency for water oxidation on TEMPO-GCE at 1.2 V vs Ag/AgCl is 59.5%. The faradaic efficiency value less than 100% can be attributed to the oxidation of carbon occurring simultaneously with water oxidation.[31,34] One should notice that this process does not affect the tip current because CO_2 cannot be reduced at a Pt electrode in aqueous media.[56] Therefore, the current measured at the SECM tip at negative potentials (curves 2-4 in Fig. 4B) is due to the reduction of H_2O_2 and O_2 rather than CO_2. Pure negative feedback was observed in a control

SECM experiment with a bare carbon substrate (data not shown).

Oxidation of primary alcohols and glycerol. TEMPO has been widely used as a molecular catalyst for alcohol oxidation in alternative energy applications and synthesis.[46,57-59] It exhibits modest activity as a homogeneous catalyst for oxidation of n-butanol in a neutral aqueous solution (Fig. S7A, the inset). A comparative study of n-butanol oxidation with several nitroxyl derivatives showed that the catalytic activity is largely affected by the driving force, i.e., the catalyst standard potential.[58] In voltage-driven catalysis with surface-bound TEMPO (Fig. S7A), the driving force is augmented by the applied anodic bias. Thus, the catalytic current density is modest at E = 0.65 V vs Ag/AgCl (at which TEMPO is fully oxidized), but becomes much higher at E = 1.2 V. Qualitatively similar voltage-assisted response can be seen at pH 13 but the catalytic activity is much higher (Fig. S7B). Consistent with previous mechanistic studies, this can be attributed to base-promoted formation of the $TEMPO^+$/alkoxide adduct.[47] A linear Tafel plot obtained for this process is shown in Fig. S3B ($E^{\circ}_{PrCHO/PrCH_2OH}$ = -0.762 V vs Ag/AgCl at pH 13 [62]).

The efficient TEMPO catalysis of ethanol oxidation has only been attained using Cu(bpy)/TEMPO co-catalyst systems[58] and a hybrid catalyst cascade architecture containing an enzyme.[60,61] We have not observed significant ethanol oxidation current either for homogeneous or voltage-assisted TEMPO catalysis at pH 7. At a higher pH, efficient voltage-assisted catalytic oxidation of ethanol occurs at the TEMPO-modified GCE (Fig. 5A). Fig. S3C shows the corresponding Tafel plot ($E^{\circ}_{CH_3CHO/CH_3CH_2OH}$ = -0.767 V vs Ag/AgCl at pH 13 [62]). Similar to water oxidation voltammograms (Figs. 2B and 2C), the apparent current density of ethanol oxidation at a TEMPO-CNE (Fig. 5B) is 2-3 orders of magnitude higher than at a TEMPO-GCE (Fig. 5A) due to the higher density of TEMPO molecules attached to the porous carbon layer.

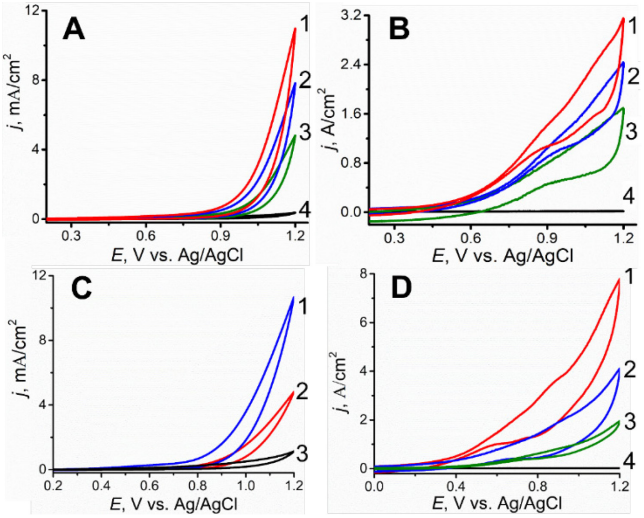

Fig. 5. Ethanol (A,B) and glycerol (C,D) oxidation catalysis by TEMPO. (A,B) Voltammograms of ethanol oxidation at (A) TEMPO-GCE and (B) TEMPO-CNE. $c_{ethanol}$, mM = 30 (1), 20 (2), and 10 (3) in 0.1 KOH. Curve 4 is the voltammogram of 20 mM ethanol at the bare GCE (A) and CNE (B). (C,D) Voltammograms of GOR at TEMPO-modified GCE (C) and CNE (D) in 0.1 M KOH. $c_{glycerol}$, mM = 10 (1), 5 (2), and 0 (3) in (C), and 20 (1, 4), 10 (2), and 5 (3) in (D). Curve 4 in (D) was recorded at the bare CNE. v = 20 mV/s.

Glycerol is a promising non-toxic, non-volatile, high energy density fuel.[63,64] The glycerol electrooxidation reaction (GOR) has typically been carried out using various precious metal based[65-67] and non-precious metal[68,69] heterogeneous catalysts. Hybrid enzymatic catalytic systems have been designed for GOR,[70,71] however, this process has not yet been carried out with a single metal-free molecular catalyst. CVs of voltage-driven molecular catalysis of GOR by surface-bound TEMPO are shown in Fig. 5C. The catalytic current is proportional to glycerol concentration, and the 11 mA/cm^2 current density at +1.2 V for $c_{glycerol}$ = 10 mM (curve 1) is about 10 times higher than the value measured for oxidation of 100 mM glycerol using 5 mM 4-amino-TEMPO as a homogeneous catalyst.[70,71] Similar to water and alcohol oxidations discussed above, voltage-driven GOR at a TEMPO-CNE electrode (Fig. 5D) produces much

larger apparent current densities (per geometrical electrode area) due to the higher density of TEMPO molecules attached to the porous carbon layer. Importantly, the GOR current measured at a bare CNE (curve 4 in Fig. 5D) is negligibly low.

Theoretical understanding of voltage-driven molecular catalysis by TEMPO. Recent DFT calculations revealed that the potential drop between the surface-bound redox species (e.g., ferrocene or $Ru(bpy)_3$ complex) and dissolved reactant molecules can contribute to the driving force for a catalytic ET reaction.[45] Unlike the outer-sphere ET processes in ref. 45, where the electrons between the surface-attached redox mediator and the reactant are transferred by tunneling, the inner-sphere water oxidation catalysis by TEMPO involves chemical bond formation.[47] The driving force for the reaction can be partitioned into the contributions from electrostatic energy and chemical potential. In addition to changing the electrostatic energy of electrons or ions, the applied voltage can modify the orbitals engaged in bond formation at the active site and affect the chemical potential.[39] We computed the plane-averaged electrostatic potentials for TEMPO-GCE at different values of the electrode potential. Because TEMPO molecules are located within the EDL, the electrostatic potential drops on both sides of the attached TEMPO (Fig. 6A). This is different from conventional molecular catalysis, where the applied electrode potential only drops between the electrode and the molecular catalyst. The potential drop between the attached TEMPO and solution increases with increasing electrode potential (Fig. 6A), providing a larger electrostatic driving force for the transfer of negatively charged reactants from solution to $TEMPO^+$ (e.g., OH^- for OER in alkaline solution).

In addition to the contribution to the electrostatic driving force, the applied electrode potential can alter the chemical bond formation. The length of the N-O bond formed when $TEMPO^+$ reacts with OH^- (d_1 in Fig. 6B) decreases from 1.645 Å at E_{PZC} to 1.509 Å at

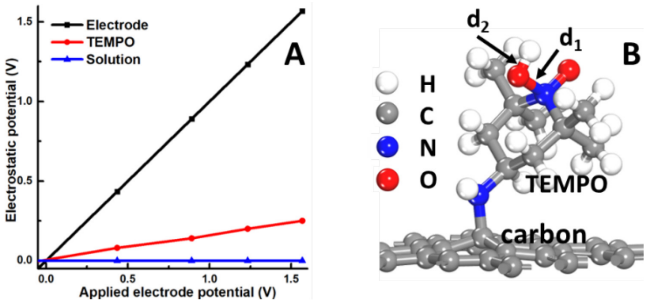

Fig. 6. Water oxidation electrocatalysis by surface-bound TEMPO in alkaline solution. (A) Plane-averaged electrostatic potentials of the carbon electrode, attached TEMPO, and solution as a function of the applied electrode potential, E (vs. E_{PZC}). (B) Structure of the attached TEMPO-OH. d_1 is the N-O bond length, and d_2 is the O-H bond length.

E = 1.22 V, indicating that the bond strength increases with the applied potential. Moreover, the O-H bond length (d_2 in Fig. 6B) slightly increases from 0.980 Å to 0.985 Å, suggesting that the applied potential may also facilitate the ensuing deprotonation of -OH. These effects can be attributed to the mixing of TEMPO orbitals with the carbon electrode, which does not occur in conventional molecular catalysis. The projected density of states (Fig. S8) shows that the orbital interaction between $TEMPO^+$ and OH^- increases at more positive E.

Unlike water oxidation, the mechanisms of alcohol oxidation catalyzed by TEMPO have been extensively studied.[59,72] In an alkaline solution, the formation of an adduct between the alcohol substrate and $TEMPO^+$ (Fig. 7A) is followed by the rate-determining intramolecular hydrogen transfer to produce the corresponding aldehyde and hydroxylamine (TEMPOH) (Fig. 7B).[73-75] The intramolecular hydrogen transfer step does not involve transfer of ions/electrons from solution, so the rate increase is due to changes in the relative chemical potentials of the products and reactants. The DFT calculated reaction free energy of this step for ethanol oxidation decreases as E becomes more positive (Fig. 7C), which is consistent with experimental observations of increased reaction rates at higher anodic potentials and can be

explained by the changes in the orbital interactions between $TEMPO^+$ and $CH_3CH_2O^-$. Strong interactions between the antibonding orbitals of $TEMPO^+$ and $CH_3CH_2O^-$ result in a bonding orbital, and the net effect is that almost one electron is transferred to the $TEMPO^+$ LUMO.[75] At higher *E* values, the orbital interactions become weaker (Fig. S9), and the distance between N and O in the intermediate (d in Fig. 7A) gets longer. Thus, our calculations show that the ethanol oxidation on TEMPO-GCE can be predominantly driven by changes in chemical potentials for the rate-determining intramolecular hydrogen transfer step.

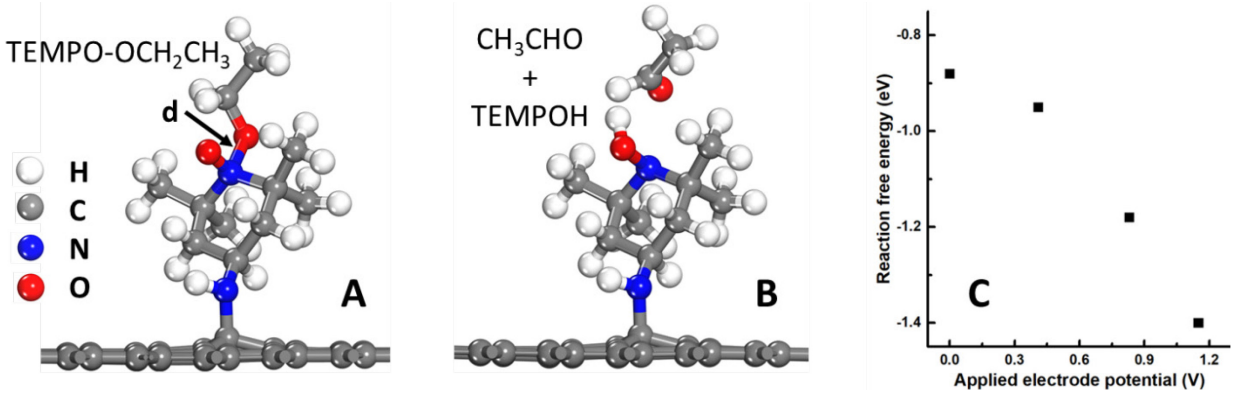

Fig. 7. Ethanol oxidation electrocatalysis by surface-bound TEMPO in alkaline solution. (A) Structure of the TEMPO-OCH_2CH_3 intermediate. (B) Formation of TEMPOH and CH_3CHO after the intramolecular hydrogen transfer. (C) Reaction free energy of the rate-determining step as a function of *E* (vs. E_{PZC}).

CONCLUSIONS

We used a recently developed concept of voltage-driven molecular catalysis to design a hybrid molecular electrocatalyst for water and alcohol oxidations by straightforward covalent attachment of metal-free (purely organic), commercially available TEMPO radical to the carbon electrode surface. A very low load and ease of recycling distinguishes it from homogeneous molecular catalysts. Unlike typical heterogeneous electrocatalysts, it is highly stable, unaffected by surface passivation and dissolution, and does not require engineering of active sites.[76] The

electrode potential contribution to the catalytic driving force results in a low onset potential and high current density at low overpotentials. It enables efficient TEMPO-mediated oxidation of water and other reactions that would not be possible if the same reagent was used as a homogeneous catalyst. Although the detailed mechanisms of water and alcohol oxidations on TEMPO-GCE have yet to be elucidated, our DFT calculations suggest both the electrostatic potential drop between the attached TEMPO and the reactant and the changes in the chemical bonds between these species contribute to the enhanced catalysis. In this way, new molecular catalysts for OER and other energy-related processes can be designed with a better stability, lower overpotential, and higher turnover numbers.

EXPERIMENTAL SECTION

Chemicals and materials. TEMPO, 4-amino-TEMPO, and KOH were purchased from Sigma-Aldrich, and hydrogen peroxide (35% w/w aqueous solution) was from Alfa Aesar. Sodium phosphate dibasic (Sigma-Aldrich, 99.95% trace metals basis) and sodium phosphate monobasic (anhydrous, Sigma-Aldrich, 99.998% trace metals basis) were used to make 0.1 M phosphate buffer (pH 7.2). Ethyl alcohol, glycerol, and n-butyl alcohol were purchased from Sigma-Aldrich. All aqueous solutions were prepared using water from Milli-Q Advantage A10 system (Millipore Corp.) equipped with Q-Gard T2 Pak, a Quantum TEX cartridge, and a VOC Pak with total organic carbon (TOC) $\leq$ 1 ppb.

Electrochemical instruments and procedures. Electrochemical experiments were carried out using a CHI 760E bipotentiostat (CH Instruments) inside a Faraday cage. In a three-electrode setup, a 1.5-mm-radius GCE (CH Instruments) or a CNE was used as a working electrode, a Pt wire was used as a counter electrode, and a commercial Ag/AgCl (1 M KCl) – as a reference electrode.

SECM setup and procedures. SECM experiments were carried out using a home-built instrument, which was described previously.[77] A homemade Teflon cell contained a four-electrode arrangement with a Pt wire counter electrode and a commercial Ag/AgCl reference electrode (CH Instruments). All experiments were carried out at room temperature (23 ± 2 °C) inside a Faraday cage. A 1.5-mm-radius TEMPO-GCE was used as a substrate electrode, and the tip – either a 3.5-μm-radius TEMPO-modified carbon fiber electrode or a 5-μm-radius Pt disk electrode – was positioned 5 μm above its surface in 0.1 M KOH solution. The substrate potential was either E_S = 0.2 V, at which the substrate current was very low, and no appreciable water oxidation occurred, or 1.2 V corresponding to significant water oxidation and peroxide oxidation current densities at TEMPO-GCE. The i_T-t curves at the TEMPO-modified carbon fiber tip were recorded at E_T = 0.8 V; and the voltammograms at the Pt tip were recorded with the potential sweep rate, v = 20 mV/s.

Fabrication of carbon nanoelectrodes. CNEs with the tip radii ~50 nm were fabricated as reported previously.[77] Briefly, nanopipettes were prepared by pulling quartz capillaries (1.0 mm o.d., 0.5 mm i.d.; Sutter Instrument Company) with a laser pipette puller (P-2000, Sutter Instruments). Carbon was deposited onto the inner pipette wall by chemical vapor deposition (CVD) at 950°C, using methane as the carbon source and argon as the protector (argon/methane: 3/5). A 1-hour deposition time was sufficient to nearly fill the nanopipettes with carbon. The electrostatic discharge protection was used in all experiments to prevent nanoscale damage to CNEs.[78] The radius value was validated, and the electrode geometry was checked by transmission electron microscopy (TEM), using a JEOL JEM-2100 instrument. The catalytic current density values for CNEs were calculated using the geometrical surface area.

Chemical modification of GCE/CNE/carbon fiber surface. 4-amino-TEMPO was immobilized on the carbon surface using a reported procedure.[50] The modification process was done by dissolving amino-TEMPO in phosphate buffer (pH 7.2) and applying +0.45 V vs. Ag/AgCl for 5 mins. 4-amino-TEMPO was attached to the electrode surface through an amine linkage. After the modification step, the electrode was washed with water. Modified electrodes showed good stability (Fig. S10) in PBS (pH 7) as well as in 0.1 M KOH (pH 13).

Computational methods. DFT calculations were performed by using the Vienna *ab initio* simulation package (VASP).[79,80] Electron exchange-correlation was represented by the functional of Perdew, Burke and Ernzerhof (PBE) of generalized gradient approximation (GGA).[81] The ion-electron interaction was described with the projector augmented wave (PAW) method.[82] The aqueous environment of the electrolyte was treated with a continuum dielectric model as implemented in the VASPsol code.[83,84] More computational details can be found in Supporting Information.

Supporting Information. Supplementary electrochemical data, CVs, and projected density of states for TEMPO-OH and TEMPO-OCH_2CH_3, Tafel plots, computational details, and COMSOL reports, including Figures S1 – S10. This material is available free of charge via the Internet at http://pubs.acs.org.

ACKNOWLEDGMENTS

The support of this work by the National Science Foundation grant CHE-1900463 (MVM) is gratefully acknowledged. GH thanks Queens College for the financial and facility support. This research used resources of the National Energy Research Scientific Computing Center, a DOE Office of Science User Facility supported by the Office of Science of the U.S. Department of Energy under Contract No. DE-AC02-05CH11231 using NERSC award BES-

ERCAP0023976.. We thank Ms. Xiang Wang and Mr. Shu Wu for preparing carbon fiber and Pt microelectrodes for SECM experiments.

COMPETING INTERESTS STATEMENT

The authors declare that they have no conflict of interest.

REFERENCES

1. Lewis, N. S.; Nocera, D. G. Powering the planet: chemical challenges in solar energy utilization. *Proc. Natl Acad. Sci. USA* **2006**, *103*, 15729–15735.
2. Hurst, J. K. Chemistry in pursuit of water oxidation catalysts for solar fuel production. *Science* **2010**, *328*, 315–316.
3. *Fuel cell catalysis, a surface science approach*; Koper, M. T. M., Ed.; Wiley, 2009, 720 p.
4. Savéant, J.-M. Molecular Catalysis of Electrochemical Reactions. Mechanistic Aspects. *Chem. Rev.* **2008**, *108*, 2348–2378.
5. Sala, X.; Romero, I.; Rodríguez, M.; Escriche, L.; Llobet, A. Molecular catalysts that oxidize water to dioxygen. *Angew. Chem. Int. Ed.* **2009**, *48*, 2842–2852.
6. Blakemore, J. D.; Crabtree, R. H.; Brudvig, Gary W. Molecular Catalysts for Water Oxidation, *Chem. Rev.* **2015**, *115*, 12974–13005.
7. Li, J.; Triana, C. A.; Wan, W.; Adiyeri Saseendran, D. P.; Zhao, Y.; Balaghi, S. E.; Heidari, S.; Patzke, G. R. Molecular and heterogeneous water oxidation catalysts: recent progress and joint perspectives. *Chem. Soc. Rev.* **2021**, *50*, 2444-2485.
8. Gersten, S. W.; Samuels, G. J.; Meyer, T. J. Catalytic oxidation of water by an oxo-bridged ruthenium dimer. *J. Am. Chem. Soc.* **1982**, *104*, 4029–4030.
9. Concepcion, J. J.; Tsai, M. K.; Muckerman, J. T.; Meyer, T. J. Mechanism of water oxidation by single-site ruthenium complex catalysts. *J. Am. Chem. Soc.* **2010**, *132*, 1545–1557.
10. Barnett, S. M.; Goldberg, K. I.; Mayer, J. M. A soluble copper-bipyridine water-oxidation electrocatalyst. *Nat. Chem.* **2012**, *4*, 498-502.
11. Limburg, J.; Vrettos, J. S.; Liable-Sands, L. M.; Rheingold, A. L.; Crabtree, R. H.; Brudvig, G. W. A functional model for O–O bond formation by the O_2-evolving complex in photosystem II. *Science* **1999**, *283*, 1524–1527.
12. Wada, T.; Tsuge, K.; Tanaka, K. Electrochemical Oxidation of Water to Dioxygen Catalyzed by the Oxidized Form of the Bis(ruthenium – hydroxo) Complex in H_2O. *Angew. Chem. Int. Ed.* **2000**, *39*, 1479–1482.
13. Sens, C.; Romero, I.; Rodriguez, M.; Llobet, A.; Parella, T.; Benet-Buchholz, J. A New Ru Complex Capable of Catalytically Oxidizing Water to Molecular Dioxygen. *J. Am. Chem. Soc.* **2004**, *126*, 7798–7799.
14. Zong, R.; Thummel, R. P. A new family of Ru complexes for water oxidation. *J. Am. Chem. Soc.* **2005**, *127*, 12802–12803.
15. Kanan, M. W.; Nocera, D. G. In situ formation of an oxygen-evolving catalyst in neutral water containing phosphate and Co^{2+}. *Science* **2008**, *321*, 1072–1075.
16. McDaniel, N. D.; Coughlin, F. J.; Tinker, L. L.; Bernhard, S. Cyclometalated iridium(III)

aquo complexes: efficient and tunable catalysts for the homogeneous oxidation of water. *J. Am. Chem. Soc.* **2008**, *130*, 210–217.
17. Duan, L.; Fischer, A.; Xu, Y.; Sun, L. Isolated Seven-Coordinate Ru(IV) Dimer Complex with [HOHOH]$^{-}$ Bridging Ligand as an Intermediate for Catalytic Water Oxidation. *J. Am. Chem. Soc.* **2009**, *131*, 10397-10399.
18. Ellis, W. C., McDaniel, N. D., Bernhard, S. & Collins, T. J. Fast water oxidation using iron. *J. Am. Chem. Soc.* **2010**, *132*, 10990–10991.
19. Schulze, M.; Kunz, V.; Frischmann, P. D.; Würthner, F. A. Supramolecular ruthenium macrocycle with high catalytic activity for water oxidation that mechanistically mimics photosystem II. *Nat. Chem.* **2016**, *8*, 576−583.
20. Yin, Q.; Tan, J. M.; Besson, C.; Geletii, Y. V.; Musaev, D. G.; Kuznetsov, A. E.; Luo, Z.; Hardcastleand, K. I.; Hill, C. L. A fast soluble carbon-free molecular water oxidation catalyst based on abundant metals. *Science* **2010**, *328*, 342–345.
21. Garrido-Barros, P.; Gimbert-Surinach, C.; Moonshiram, D.; Picón, A.; Monge, P.; Batista, V. S.; Llobet, A. Electronic π- delocalization boosts catalytic water Oxidation by Cu(II) molecular catalysts heterogenized on graphene sheets. *J. Am. Chem. Soc.* **2017**, *139*, 12907−12910.
22. Lebedev, D.; Pineda-Galvan, Y.; Tokimaru, Y.; Fedorov, A.; Kaeffer, N.; Copéret, C.; Pushkar, Y. The key Ru^{V}=O intermediate of site-isolated mononuclear water oxidation catalyst detected by in situ X-ray absorption spectroscopy. *J. Am. Chem. Soc.* **2018**, *140*, 451−458.
23. Gil-Sepulcre, M.; Linder, J. O.; Schindler, D.; Velasco, L.; Moonshiram, D.; Rüdinger, O.; Stepanenko, V.; Solano, E.; Würthner, F.; Llobet, A. Surface promoted evolution of Ru-bda coordination oligomers boost the efficiency of water oxidation molecular electroanodes. *J. Am. Chem. Soc.* **2021**, *143*, 11651−11661.
24. Hoque, Md. A.; Gil-Sepulcre, M.; de Aguirre, A.; Elemans, J. A. A. W.; Moonshiram, D.; Matheu, R.; Shi, Y.; Benet-Buchholz, J.; Sala, X.; Malfois, M.; Solano, E.; Lim, J.; Garzón-Manjón, A.; Scheu, C.; Lanza, M.; Maseras, F.; Gimbert-Suriñach, C.; Llobet, A. Water oxidation electrocatalysis using ruthenium coordination oligomers adsorbed on multiwalled carbon nanotubes. *Nat. Chem.* **2020**, *12*, 1060−1066.
25. Schindler, D.; Gil-Sepulcre, M.; Lindner, J. O.; Stepanenko, V.; Moonshiram, D.; Llobet, A.; Würthner, F. Efficient electrochemical water oxidation by a trinuclear Ru(bda) macrocycle immobilized on multi-walled carbon nanotube electrodes. *Adv. Energy Mater.* **2020**, *10*, 2002329.
26. Wang, L.; Fan, K.; Daniel, Q.; Duan, L.; Li, F.; Philippe, B.; Rensmo, H.; Chen, H.; Sun, J.; Sun, L. Electrochemical driven water oxidation by molecular catalysts in situ polymerized on the surface of graphite carbon electrode. *Chem. Commun.* **2015**, *51*, 7883−7886.
27. Joya, K. S.; Subbaiyan, N. K.; D'Souza, F.; de Groot, H. J. M. Surface-immobilized single-site iridium complexes for electrocatalytic water Splitting. *Angew. Chem., Int. Ed.* **2012**, *51*, 9601−9605.
28. Li, X.; Lei, H.; Liu, J.; Zhao, X.; Ding, S.; Zhang, Z.; Tao, X.; Zhang, W.; Wang, W.; Zheng, X.; Cao, R. Carbon nanotubes with cobalt corroles for hydrogen and oxygen evolution in pH 0−14 solutions. *Angew. Chem., Int. Ed.* **2018**, *57*, 15070−15075.
29. Costentin, C.; Porter, T. R.; Savéant, J.-M. Conduction and reactivity in heterogeneous-molecular catalysis: new insights in water oxidation catalysis by phosphate cobalt oxide

films. *J. Am. Chem. Soc.* **2016**, *138*, 5615−5622.
30. Luo, S.-X. L.; Liu, R. Y.; Lee, S.; Swager, T. M. Electrocatalytic isoxazoline-nanocarbon metal complexes. *J. Am. Chem. Soc.* **2021**, *143*, 10441−10453.
31. Mirzakulova, E.; Khatmullin, R.; Walpita, J.; Corrigan, T.; Vargas-Barbosa, N. M.; Vyas, S.; Oottikkal, S.; Manzer, S. F.; Hadad, C. M.; Glusac, K. D. Electrode-assisted catalytic water oxidation by a flavin derivative. *Nat. Chem.* **2012**, *4*, 794−801.
32. Yang, X.; Walpita, J.; Mirzakulova, E.; Oottikkal, S.; Hadad, C. M.; Glusac, K. D. Mechanistic studies of electrode-assisted catalytic oxidation by flavinium and acridinium cations. *ACS Catal.* **2014**, *4*, 2635−2644.
33. Wu, Y.; Klein, V.; Killian, M. S.; Behling, C.; Chea, S.; Tokoeka, S. B.; Bachmann, J. Novel fully organic water oxidation electrocatalysts: a quest for simplicity. *ACS Omega* **2018**, *3*, 2602−2608.
34. Li, H.; Xian, F.; Zhang, M.-T. Metal-free electrocatalyst for water oxidation initiated by hydrogen atom transfer. *ACS CATA.* **2021**, *11*, 68−73.
35. Lutterman, D. A.; Surendranath, Y.; Nocera, D. G. A self-healing oxygen evolving catalyst. *J. Am. Chem. Soc.* **2009**, *131*, 3838–3839.
36. Yang, Y.; Peltier, C. R.; Zeng, R.; Schimmenti, R.; Li, Q.; Huang, X.; Yan, Z.; Potsi, G.; Selhorst, R.; Lu, X.; Xu, W.; Tader, M.; Soudackov, A. V.; Zhang, H.; Krumov, M.; Murray, E.; Xu, P.; Hitt, J.; Xu, L.; Ko, H.-Y.; Ernst, B. G.; Bundschu, C.; Luo, A.; Markovich, D.; Hu, M.; He, C.; Wang, H.; Fang, J.; DiStasio, R. A., Jr.; Kourkoutis, L. F.; Singer, A.; Noonan, K. J. T.; Xiao, L.; Zhuang, L.; Pivovar, B. S.; Zelenay, P.; Herrero, E.; Feliu, J. M.; Suntivich, J.; Giannelis, E. P.; Hammes-Schiffer, S.; Arias, T.; Mavrikakis, M.; Mallouk, T. E.; Brock, J. D.; Muller, D. A.; DiSalvo, F. J.; Coates, G. W.; Abruña, H. D. Electrocatalysis in Alkaline Media and Alkaline Membrane-Based Energy Technologies. *Chem. Rev.* **2022**, *122*, 6117−6321.
37. Wu, L.; Nayak, A.; Shao, J.; Meyer, T. J. Crossing the bridge from molecular catalysis to a heterogenous electrode in electrocatalytic water oxidation. *Proc. Natl. Acad. Sci. USA* **2019**, **116**, 11153-11158.
38. Nong, H. N.; Falling, L. J.; Bergmann, A.; Klingenhof, M.; Tran, H. P.; Spöri, C.; Mom, R.; Timoshenko, J.; Zichittella, G.; Knop-Gericke, A.; Piccinin, S.; Pérez-Ramírez, J.; Cuenya, B. R.; Schlögl, R.; Strasser, P.; Teschner, D.; Jones, T. E. Key role of chemistry versus bias in electrocatalytic oxygen evolution. *Nature* **2020**, *587*, 408–413.
39. Boettcher, S. W.; Surendranath, Y. Heterogeneous electrocatalysis goes chemical. *Nat. Catal.* **2021**, *4*, 4–5.
40. Bates, J. S.; Biswas, S.; Suh, S.-E.; Johnson, M. R.; Mondal, B.; Root, T. W.; Stahl, S. S. Chemical and electrochemical O_2 reduction on earth-abundant M-N-C catalysts and implications for mediated electrolysis. *J. Am. Chem. Soc.* **2022**, *144*, 922-927.
41. Oh, S.; Gallagher, J. R.; Miller, J. T.; Surendranath, Y. Graphite-conjugated rhenium catalysts for carbon dioxide reduction. *J. Am. Chem. Soc.* **2016**, *138*, 1820−1823.
42. Jackson, M. N.; Surendranath, Y. Molecular control of heterogeneous electrocatalysis through graphite conjugation. *Acc. Chem. Res.* **2019**, *52*, 3432–3441.
43. Jackson, M. N.; Oh, S.; Kaminsky, C. J.; Chu, S. B.; Zhang, G.; Miller, J. T.; Surendranath, Y. Strong Electronic Coupling of Molecular Sites to Graphitic Electrodes via Pyrazine Conjugation. *J. Am. Chem. Soc.* **2018**, *140*, 1004–1010.
44. Kaminsky, C. J.; Weng, S.; Wright, J.; Surendranath, Y. Adsorbed cobalt porphyrins act like metal surfaces in electrocatalysis. *Nat. Catal.* **2022**, *5*, 430-442.

45. Barman, K.; Wang, X.; Jia, R.; Askarova, G.; Hu, G.; Mirkin, M. V. Voltage-driven molecular catalysis of electrochemical reactions. *J. Am. Chem. Soc.* **2021**, *143*, 17344−17347.
46. Yan, M.; Kawamata, Y.; Baran, P. S. Synthetic organic electrochemical methods since 2000: on the verge of a renaissance. *Chem. Rev.* **2017**, *117*, 13230–13319.
47. Nutting, J. E.; Rafiee, M.; Stahl, S. S. Tetramethylpiperidine N-oxyl (TEMPO), phthalimide N-oxyl (PINO), and related N-oxyl species: electrochemical properties and their use in electrocatalytic reactions. *Chem. Rev.* **2018**, *118*, 4834−4885.
48. Asmus, K. D.; Nigam, S.; Willson, R. L. Kinetics of nitroxyl radical reactions. A pulse-radiolysis conductivity study. *Int. J. Radiat. Biol. Relat. Stud. Phys., Chem. Med.* **1976**, *29*, 211−219.
49. Fish, J. R.; Swarts, S. G.; Sevilla, M. D.; Malinski, T. Electrochemistry and spectroelectrochemistry of nitroxyl free radicals. *J. Phys. Chem.* **1988**, *92*, 3745−3751.
50. Geneste, F.; Moinet, C. Electrochemically linking TEMPO to carbon via amine bridges. *New J. Chem.* **2005**, *29*, 269−271.
51. Semmelhack, M. F.; Schmid, C. R. Nitroxyl-mediated electrooxidation of amines to nitriles and carbonyl compounds. *J. Am. Chem. Soc.* **1983**, *105*, 6732−6734.
52. Kishioka, S.-y.; Ohki, S.; Ohsaka, T.; Tokuda, K. Reaction mechanism and kinetics of alcohol oxidation at nitroxyl radical modified electrodes. *J. Electroanal. Chem*. **1998**, *452*, 179−186.
53. Rafiee, M.; Karimi, B.; Alizadeh, S. Mechanistic study of the electrocatalytic oxidation of alcohols by TEMPO and NHPI. *ChemElectroChem* **2014**, *1***,** 455−462.
54. Bae, J. H.; Wang, D.; Hu, K.; Mirkin, M. V. Surface charge effects on voltammetry in carbon nanocavities. *Anal. Chem.* **2019**, *91*, 5530–5536.
55. Abdellaoui, S.; Knoche, K. L.; Lim, K.; Hickey, D. P.; Minteer, S. D. TEMPO as a promising electrocatalyst for the electrochemical oxidation of hydrogen peroxide in bioelectronic applications. *J. Electrochem. Soc.* **2016**, *163*, H3001-H3005.
56. Tomita, Y.; Teruya, S.; Koga, O.; Hori, Y. Electrochemical reduction of carbon dioxide at a platinum electrode in acetonitrile-water mixtures. Journal of The Electrochemical Society 2000, 147, 4164-4167
57. Vogler, T.; Studer, A. Applications of TEMPO in synthesis. *Synthesis* **2008**, *13*, 1979−1993.
58. Rafiee, M.; Miles, K. C.; Stahl, S. S. Electrocatalytic alcohol oxidation with TEMPO and bicyclic nitroxyl derivatives: driving force trumps steric effects. *J. Am. Chem. Soc*. **2015**, *137*, 14751−14757.
59. Badalyan, A.; Stahl, S. S. Cooperative Electrocatalytic alcohol oxidation with electron-proton-transfer mediators. *Nature* **2016**, *535*, 406−410.
60. Franco, J. H.; Neto, S. A.; Hickey, D. P.; Minteer, S. D.; de Andrade, A. R. Hybrid catalyst cascade architecture enhancement for complete ethanol electrochemical oxidation. *Biosens. Bioelectron.* **2018**, *121*, 281–286.
61. Franco, J. H.; Klunder K. J.; Lee, J.; Russell, V.; de Andrade, A. R.; Minteer, S. D. Enhanced electrochemical oxidation of ethanol using a hybrid catalyst cascade architecture containing pyrene-TEMPO, oxalate decarboxylase and carboxylated multi-walled carbon nanotube. *Biosensors and Bioelectronics* **2020**, *154*, 112077.

62. Speelman, A. L.; Gerken, J. B.; Heins, S. P.; Wiedner, E. S.; Stahl, S. S.; Appel, A. M. Determining overpotentials for the oxidation of alcohols by molecular electrocatalysts in non-aqueous solvents. *Energy Environ. Sci.* **2022**, *15*, 4015−4024.
63. Arechederra, R. L.; Treu, B. L.; Minteer, S. D. Development of glycerol/O_2 biofuel cell. *J. Power Sources* **2007**, *173*, 156−161.
64. Fan, L.; Liu, B.; Liu, X.; Senthilkumar, N.; Wang, G.; Wen, Z. Recent progress in electrocatalytic glycerol oxidation. *Energy Technol.* **2020**, *9*, 2000804.
65. Mello, G. A.; Busó-Rogero, C.; Herrero, E.; Feliu, J. M. Glycerol electrooxidation on Pd modified Au surfaces in alkaline media: Effect of the deposition method. *J. Chem. Phys.* **2019**, *150*, 041703.
66. Yang, F.; Ye, J.; Yuan, Q.; Yang, X.; Xie, Z.; Zhao, F.; Zhou, Z.; Gu, L.; Wang, X. Ultrasmall Pd-Cu-Pt trimetallic twin icosahedrons boost the electrocatalytic performance of glycerol oxidation at the operating temperature of fuel cells. *Adv. Funct. Mater.* **2020**, *30*, 1908235.
67. Li, T.; Harrington, D. A. An overview of glycerol electrooxidation mechanisms on Pt, Pd and Au. *ChemSusChem* **2021**, *14*, 1472-1495.
68. Schünemann, S.; Schüth, F.; Tüysüz, H. Selective glycerol oxidation over ordered mesoporous copper aluminum oxide catalysts. *Catal. Sci. Technol*. **2017**, *7*, 5614−5624.
69. Du, J.; Xie, A.; Zhu, S.; Xiong, Z.; Yu, X.; Yang, F.; Tao, Y.; Luo, S. 3D flower-like $CoNi_2S_4$/polyaniline with high performance for glycerol electrooxidation in an alkaline medium. *New J. Chem*. **2019**, *43*, 10366−10375.
70. Hickey, D. P.; McCammant, M. S.; Giroud, F.; Sigman, M. S.; Minteer, S. D. Hybrid enzymatic and organic electrocatalytic cascade for the complete oxidation of glycerol. *J. Am. Chem. Soc.* **2014**, *136*, 15917–15920.
71. Macazo, F. C.; Hickey, D. P.; Abdellaoui, S.; Sigman, M. S.; Minteer, S. D. Polymer-immobilized, hybrid multi-catalyst architecture for enhanced electrochemical oxidation of glycerol. *Chem. Commun*. **2017**, *53*, 10310–10313.
72. Semmelhack, M. F.; Chou, C. S.; Cortes, D. A. Nitroxyl-mediated electrooxidation of alcohols to aldehydes and ketones. *J. Am. Chem. Soc.* **1983**, *105*, 4492−4494.
73. Semmelhack, M. F.; Schmid, C. R.; Cortés, D. A. Mechanism of the oxidation of alcohols by 2,2,6,6-tetramethylpiperdine nitrosonium cation. *Tetrahedron Lett.* **1986**, *27*, 1119−1122.
74. Bailey, W. F.; Bobbitt, J. M.; Wiberg, K. B. Mechanism of the oxidation of alcohols by oxoammonium cations. *J. Org. Chem*. **2007**, *72*, 4504−4509.
75. Michel, C.; Belanzoni, P.; Gamez, J.; Reedijk, J.; Baerends, E. J. Activation of the C−H bond by electrophilic attack: theoretical study of the reaction mechanism of the aerobic oxidation of alcohols to aldehydes by the $Cu(bipy)^{2+}$/2,2,6,6-tetramethylpiperidinyl-1-oxy cocatalyst system. *Inorg. Chem*. **2009**, *48*, 11909−11920.
76. Zaera, F. Designing Sites in Heterogeneous Catalysis: Are we reaching selectivities competitive with those of homogeneous catalysts? *Chem. Rev.* **2022**, *122*, 8594-8757.
77. Li, Y.; Hu, K.; Yu, Y.; Rotenberg, S. A.; Amatore, C.; Mirkin, M. V. Direct electrochemical measurements of reactive oxygen and nitrogen species in nontransformed and metastatic human Breast Cells. *J. Am. Chem. Soc.* **2017**, *139*, 13055−13062.
78. Nioradze, N.; Chen, R.; Kim, J.; Shen, M.; Santhosh, P.; Amemiya, S. Origins of nanoscale damage to glass-sealed platinum electrodes with submicrometer and nanometer size. *Anal. Chem.* **2013**, *85*, 6198−6202.

79. Kresse, G.; Furthmüller, J. Efficient iterative schemes for Ab-Initio total-energy calculations using a plane-wave basis set. *Phys. Rev. B*. **1996**, *54*, 11169-11186.
80. Kresse, G.; Furthmüller, J. Efficiency of Ab-Initio total energy calculations for metals and semiconductors using a plane-wave basis set. *Comput. Mater. Sci*. **1996**, *6*, 15-50.
81. Perdew, J. P.; Burke, K.; Ernzerhof, M. Generalized gradient approximation made simple. *Phys. Rev. Lett*. **1996**, *77*, 3865.
82. Blöchl, P. E. Projector Augmented-Wave Method. Phys. Rev. B. **1994**, *50*, 17953-17979.
83. Mathew, K.; Sundararaman, R.; Letchworth-Weaver, K.; Arias, T.; Hennig, R. G. Implicit solvation model for density-functional study of nanocrystal surfaces and reaction pathways. *J. Chem. Phys*. **2014**, *140,* 084106.
84. Mathew, K.; Kolluru, V. C.; Mula, S.; Steinmann, S. N.; Hennig, R. G. Implicit self-consistent electrolyte model in Plane-Wave Density-Functional Theory. *J. Chem. Phys*. **2019**, *151*, 234101.

For TOC only

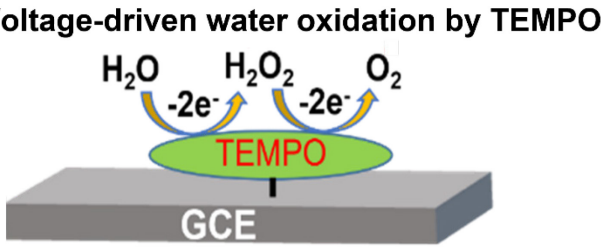
Voltage-driven water oxidation by TEMPO
H2O
H2O2
O2
-2e-
-2e-
TEMPO
GCE